Isolation Effects in Single- and Dual-Plane VLSI Interconnects

LAWRENCE CARIN AND KEVIN J. WEBB, MEMBER, IEEE

Abstract—**The issue of interline coupling in high-speed VLSI interconnects is addressed. A full-wave-based technique is used to numerically solve for the modes and hence the line voltages and currents for multiconductor microstrip. The accuracy of these results is compared with time-domain experimental data. Isolation lines placed between signal lines and grounded at both ends are considered as a means of significantly reducing crosstalk. It is shown that the performance of such lines depends on several factors such as relative mode velocities, signal rise and fall times, and line length. These points are illuminated by considering the effects of isolation lines in two geometries of interest in high-speed integrated circuits. On the basis of these results one can determine the usefulness of isolation lines for a given geometry.**

I. INTRODUCTION

THERE ARE several factors that dictate the degree of interline coupling on interconnects. As the interline spacing between the lines becomes small relative to the distance to the ground or reference line, interline coupling will increase. If the medium is homogeneous, the N TEM modes (for $N+1$ lines) will all propagate at the same speed; thus the signals on the various conductors will not change as they propagate down the transmission lines until they encounter a discontinuity or termination. At this point the line voltages and currents will change according to the port boundary conditions. For interconnects in a homogeneous medium, the degree of interline coupling is dictated solely by the geometry's cross section (primarily the interline spacing) and boundary conditions. Thus the interline coupling for a given set of boundary and initial conditions can be reduced by simply increasing the interline spacing. For interconnects embedded in an inhomogeneous medium, the degree of interline coupling is dictated by more variables than just the geometry's cross section. Since the N quasi-TEM modes will in general propagate at N different velocities, such factors as signal rise and fall time as well as line length become important.

Manuscript received August 22, 1988; revised November 29, 1989. This work was supported in part by grants from the Semiconductor Research Corporation under Contract 88-DJ-130 and Martin Marietta Laboratories.

L. Carin was with the Department of Electrical Engineering, University of Maryland, College Park, MD 20742. He is now with the Electrical Engineering and Computer Science Department, Polytechnic University, Farmingdale, NY 11735.

K. J. Webb was with the Department of Electrical Engineering, University of Maryland, College Park, MD 20742. He is now with the School of Electrical Engineering, Purdue University, West Lafayette, IN 47907.

IEEE Log Number 8933768.

A technique which can be employed to reduce crosstalk is the placement of isolation or shield lines between the various signal lines of interest. These isolation lines are usually grounded at both ends and run the length of the interconnects. The addition of grounded shield lines adds to the complexity of fabrication due to the vias (or perhaps air bridges) that are required at both ends to connect the isolation line to ground. For this reason isolation lines with open-circuit terminations were also examined in the course of this work, and for the cases studied they were found not to be as effective as grounded shield lines in reducing crosstalk (for coupled voltage or current). This paper will therefore concentrate on isolation lines with grounded terminations. Isolation lines with grounded terminations have been examined by several authors [1]–[4] with varying conclusions as to their usefulness. In this work it will be shown that the performance of such isolation lines depends on the geometry in which they are employed as well as on the signal speeds used. The emphasis will be on interconnects embedded in an inhomogeneous medium; however, it should be noted that such lines could also be used in a homogeneous medium to act as a shield between signal lines.

Interconnects can be accurately modeled as multiconductor microstrip embedded in an inhomogeneous dielectric. Historically multiconductor microstrips have been analyzed almost exclusively using the TEM approximation for the microstrip modes [1], [2], [4]–[11]. As the speeds of signals on the interconnects continue to increase, a full-wave analysis is required to provide an important benchmark solution [3], [12]–[20]. In this work the full-wave analysis of multiconductor microstrip is performed using a spectral-domain formulation [14]–[16]. Since this approach is well known, only the relevant details are outlined. The spectral-domain technique and the method used to simulate signal propagation on terminated multiconductor microstrip are discussed in Section II. Results from the theoretical technique are compared with experimental results in Section III. A simple interconnect structure is discussed in detail in Section IV to gain insight into the main mechanisms that influence interline coupling. The ideas from this special case are then used in Section V to help describe the effects of isolation lines in practical systems. Example results are presented for interconnects on GaAs substrates (common in MMIC) and for intercon-

0018-9480/90/0400-0396$01.00

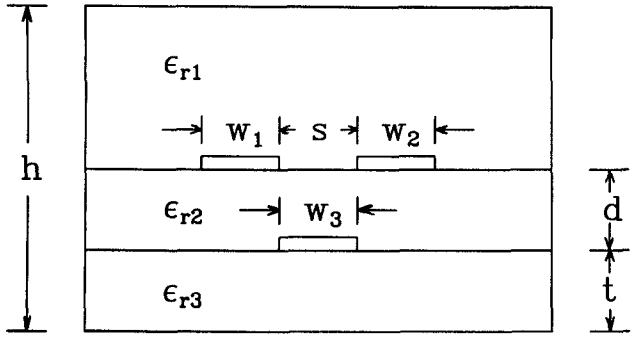

Fig. 1. Example shielded multiconductor microstrip cross section.

nects embedded in a $Si-SiO_2$ substrate (with applications in silicon-based VLSI circuits). Several geometrical parameters are varied to show their effects on the performance of grounded isolation lines. Using results from the frequency-dependent multiconductor microstrip solution, the effects of dispersion are also addressed for very high speed pulses.

II. Formulation

The spectral-domain technique [14]–[16] is used for the frequency-dependent analysis of multiple microstrip lines. Consider the multiconductor shielded microstrip geometry illustrated in Fig. 1. The current on each line for a given mode is defined as

$$i_{zlm} = \int_l J_{zlm}\, dx \tag{1}$$

where J_{zlm} is the longitudinal component of surface current density on line l for mode m. The current of interest flows in the longitudinal direction (there is also an x-directed current density) and the integral is taken perpendicular to this (along the x direction) across the strip's width. Since the modes are in general hybrid, the voltage of a given strip relative to ground cannot be uniquely defined as a line integral of electric field. Therefore, the voltage on each line for a given mode is defined indirectly by relating the line current to voltage through a modal characteristic impedance [16]–[18]. The definition of modal impedance used in this work has recently been proposed in [17]. Let the N-dimensional eigencurrent $\boldsymbol{I}_m$ for mode m consist of components i_{zlm} (the longitudinal currents on all lines for a given mode m) and the N-dimensional eigenvoltage $\boldsymbol{V}_m$ for mode m consist of components $v_{lm} = i_{zlm}Z_{lm}$, where Z_{lm} is the modal impedance for line l and mode m. In a TEM system the N eigencurrents and eigenvoltages satisfy [17]

$$\boldsymbol{V}_m^T \boldsymbol{I}_n = 2P_m \delta_{mn} \tag{2}$$

where P_m is the time-averaged power for mode m, δ_{mn} is the Kronecker delta, and the superscript T represents the transpose operation. This represents a set of $N \times N$ linear equations to solve for the $N \times N$ unknown modal impedances. The eigencurrents and time-averaged powers for each mode are calculated at each frequency using a full-wave approach such as the spectral-domain technique. This definition of modal impedance has several advantages [17], [18] over the commonly used partial-power definition [16].

The N modes are a complete set in the circuit sense and therefore can be superposed to represent any distribution of line voltages and currents (with $e^{j\omega t}$ suppressed):

$$i_{lT}(z) = \sum_{m=1}^{N} i_{zlm}\left(a_m^{(+)} e^{-jk_{zm}z} - a_m^{(-)} e^{jk_{zm}z}\right) \tag{3}$$

$$v_{lT}(z) = \sum_{m=1}^{N} i_{zlm} Z_{lm}\left(a_m^{(+)} e^{-jk_{zm}z} + a_m^{(-)} e^{jk_{zm}z}\right) \tag{4}$$

for $l = 1, 2, \cdots, N$, where $v_{lT}(z)$ and $i_{lT}(z)$ are the total voltage and current, respectively, on line l, and k_{zm} is the frequency-dependent propagation constant for mode m. Signal propagation is described by applying appropriate boundary conditions to (3) and (4), thus defining the coefficients $a_m^{(+)}$ and $a_m^{(-)}$ for each mode m. Arbitrary signals can be considered by applying proper weighting to each frequency component (dictated by the Fourier transform of the excitation) and using the inverse Fourier transform to obtain the time-domain representation. This is efficiently done by employing the fast Fourier transform algorithm (FFT). In this way the signal is represented at discrete time intervals as it propagates.

III. Experimental Results

Since digital VLSI circuits frequently require pulses to travel in a multiple conductor transmission line environment, an experiment was performed to study pulse propagation on four coupled microstrip lines on a single plane. A similar experiment was performed in [4]. The lines in the experiment were 0.254 mm wide, separated by 0.127 mm, and located on a 0.127-mm-thick Duroid ($\epsilon_r = 4.0$) substrate over a ground plane. A single pulse was sent down one of the two outermost lines and the response at the end of all lines was observed on a high-speed storage oscilloscope. The signals were measured and the driven line excited by using SMA coaxial connectors which had diameters much larger than the desired strip separations. Therefore, to connect the microstrip to the SMA connectors the lines had to be decoupled (separated) at both ends. This was done with a 7.62 cm linear transition region at both ends of the lines over which the strips were gradually decoupled. The lines were coupled (separated by 0.127 mm) over a 30.48 cm length. A 50 Ω line is approximately 0.254 mm wide on the substrate used; therefore when the lines are decoupled, each has a characteristic impedance of approximately 50 Ω. Thus, a good match was achieved between the 50 Ω coaxial connectors and the decoupled lines. Results are plotted in Fig. 2 for the voltages at the outputs of the four lines. Since the lines were decoupled (widely separated) at the two ends and well matched at the output, the loads at the inputs of the nondriven lines (at the ends of the tapers, far from the tightly coupled segment of the geometry) did not affect the measured voltages. It should be noted that some errors were incurred

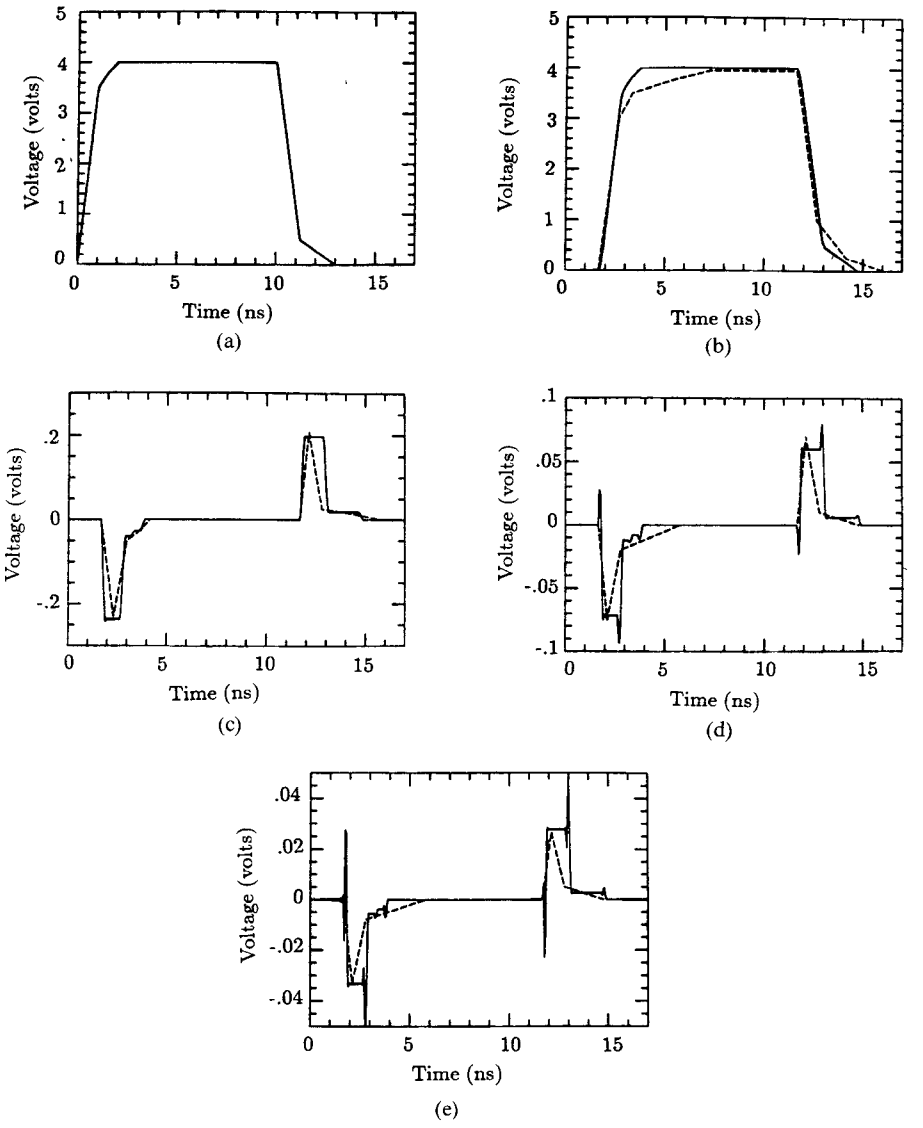

Fig. 2. Experimental and theoretical results for voltages at the output of four-line microstrip. The geometry is described in the text. Label the four lines 1 to 4 from left to right. Line 1 is driven by (a) and the outputs of lines 1 through 4 are (b) through (e), respectively. Solid line, theory; dashed, experiment.

during the conversion of the experimentally determined photographs into the figures shown; the agreement between theory and experiment is actually better than represented in Fig. 2.

Since the lines used in the experiment were well matched at the output (no reflection), they are analyzed numerically by considering semi-infinite lines. Thus, only positive propagating modes are considered in (3) and (4) and the modal coefficients for these positively propagating modes are determined by the boundary conditions at $z = 0$. Voltage boundary conditions on the inputs of the four lines are used to define the four forward propagating mode coefficients in (4). The driven line is excited numerically with a pulse corresponding to that used in the experiment. The voltages on the nondriven lines at the source end are set to zero in the analysis. This is because, as mentioned above, the coax-to-microstrip connectors used in the experiment required the strips to be decoupled at the input and output ports. The voltages on the semi-infinite lines are calculated as a function of time at $z = 30.48$ cm (using (4) in conjunction with the FFT), corresponding to the length over which the lines were coupled in the experiment. Since the rise and fall time of the source was 1 ns, the modal speeds (ω/k_{zm}), currents, and characteristic impedances were assumed constant with frequency in the calculation. One notices the effects of Gibbs' phenomena on the theoretical results (especially in Fig. 2(d) and (e)) due to the finite number of terms used in the FFT with a rectangular window.

IV. Crosstalk Characterization

The usefulness of isolation lines depends on the system in which they are incorporated. To emphasize several key factors of interest when analyzing crosstalk, a special case is studied. The example is very simple but it addresses many of the major effects in interline coupling.

Consider a system of two symmetrically situated semi-infinite microstrip transmission lines over a ground plane and assume that dispersion can be ignored. Let the lines be

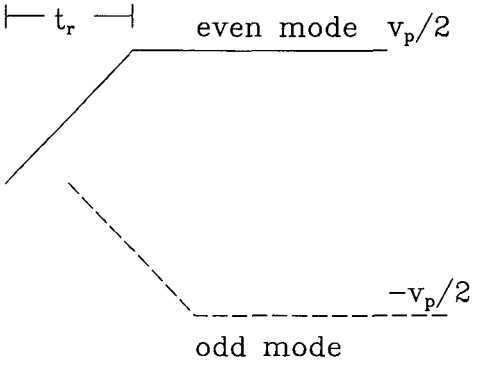

Fig. 3. Even- and odd-mode voltages on the nondriven line as a function of time at a position $z > 0$. In this figure the even mode is faster than the odd mode.

excited such that one line is driven by a step voltage source with linear rise time t_r (0 to 100%) and peak voltage v_p. The voltage on line 2 at $z = 0$ is set to zero (grounded) but there will be an induced current signal. As the signal propagates away from the source ($z > 0$), a coupled voltage will appear on the nondriven line if the two mode velocities are unequal. By examining Fig. 3, one can see that at any point $z \geq 0$, the maximum absolute value of voltage crosstalk on line 2 is

$$|V_{\max}(z,t_r)| = \frac{z}{t_r} v_p \frac{\left|\sqrt{\epsilon_{\text{eff1}}} - \sqrt{\epsilon_{\text{eff2}}}\right|}{2c} \quad \text{for } \frac{z}{t_r} \leq \frac{c}{\left|\sqrt{\epsilon_{\text{eff1}}} - \sqrt{\epsilon_{\text{eff2}}}\right|}$$

$$|V_{\max}(z,t_r)| = \frac{v_p}{2} \quad \text{for } \frac{z}{t_r} \geq \frac{c}{\left|\sqrt{\epsilon_{\text{eff1}}} - \sqrt{\epsilon_{\text{eff2}}}\right|} \tag{5}$$

where the two modes have effective dielectric constants ϵ_{eff1} and ϵ_{eff2} and c is the speed of light in a vacuum. The above equation gives insight into the parameters of interest when considering isolation lines: relative mode velocities, line lengths, and signal rise and fall times. A parameter of importance which is not emphasized in the above equations is the dependence on interline spacing. The amount of coupled current on line 2 at $z = 0$ will be dictated by the line spacing. If the lines are embedded in a homogeneous medium $\epsilon_{\text{eff1}} = \epsilon_{\text{eff2}}$, and therefore the voltage on line 2 remains zero until a termination is encountered. However, the current amplitude on line 2 will depend greatly on interline spacing and will become larger as the line spacing decreases. The effect of interline spacing on crosstalk is implied in (5) for an inhomogeneous medium, however, since the difference between ϵ_{eff1} and ϵ_{eff2} increases as the lines become more tightly coupled. The insight gained from this simple example is now applied to the analysis of interconnects used in high-speed integrated circuits.

V. Examples

In this section two systems of interest in high-speed integrated circuits are considered. First, interconnects over a GaAs substrate are analyzed, followed by a study of interconnects in a Si–SiO_2 environment. Shield lines which are grounded at both ends are investigated as a means of significantly reducing crosstalk.

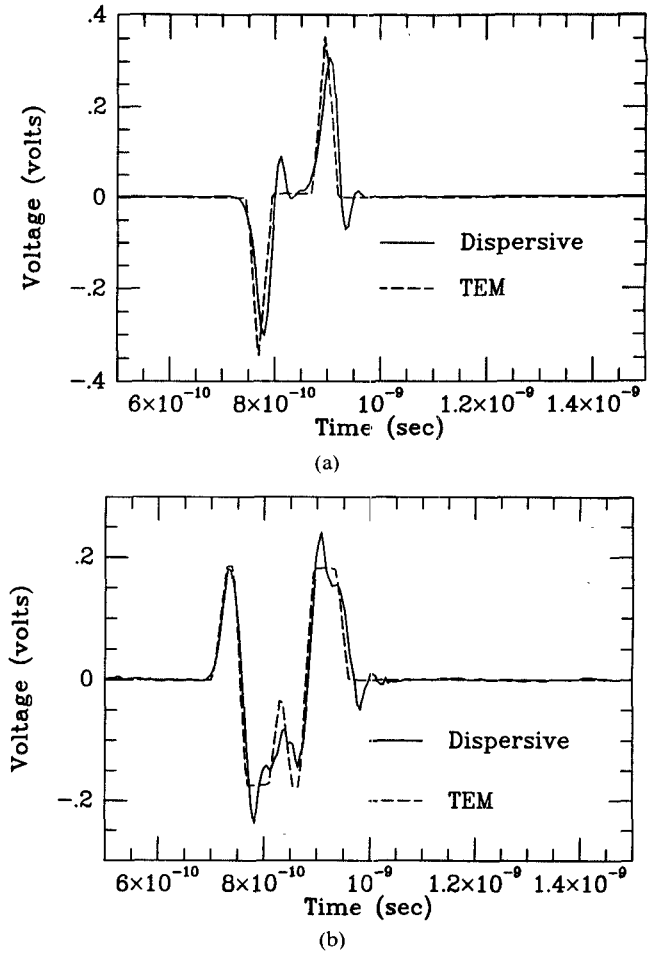

Fig. 4. Isolation results for 7.5-cm-long, 0.254-mm-wide lines on 0.127-mm-thick GaAs substrate ($\epsilon_r = 13$). Results are for (a) two lines separated by 0.508 mm and for (b) three lines separated by 0.127 mm. In (b) the middle line is grounded at both ends and for both cases the outer lines have 50 Ω source impedances and are terminated in 20 fF capacitors. One outer line is driven by a 1 V pulse with 25 ps rise and fall times and 100 ps width. All voltages are across the capacitors of the coupled line (nondriven outer line).

A. GaAs Substrate

Two lines on top of a GaAs ($\epsilon_r = 13$) substrate with a ground plane on the bottom surface are analyzed with and without the addition of a grounded shield line between them. Each of the two signal lines is terminated in a 20 fF capacitor, simulating the gate of a FET. Line 1 is driven by a 1 V peak voltage pulse with 25 ps rise (0 to 100%) and fall time and 100 ps width (at peak); line 2 is not driven and has a 50 Ω resistor placed at its input port. The source has a 50 Ω impedance. Two substrate thicknesses are considered; therefore the time-dependent coupling results are presented in two sets (each set considers a different substrate thickness). The first set of data, Fig. 4(a) and (b), is for a 0.127-mm-thick substrate and the second set, Fig. 5(a) and (b), is for a 0.381-mm-thick substrate. Part (a) of

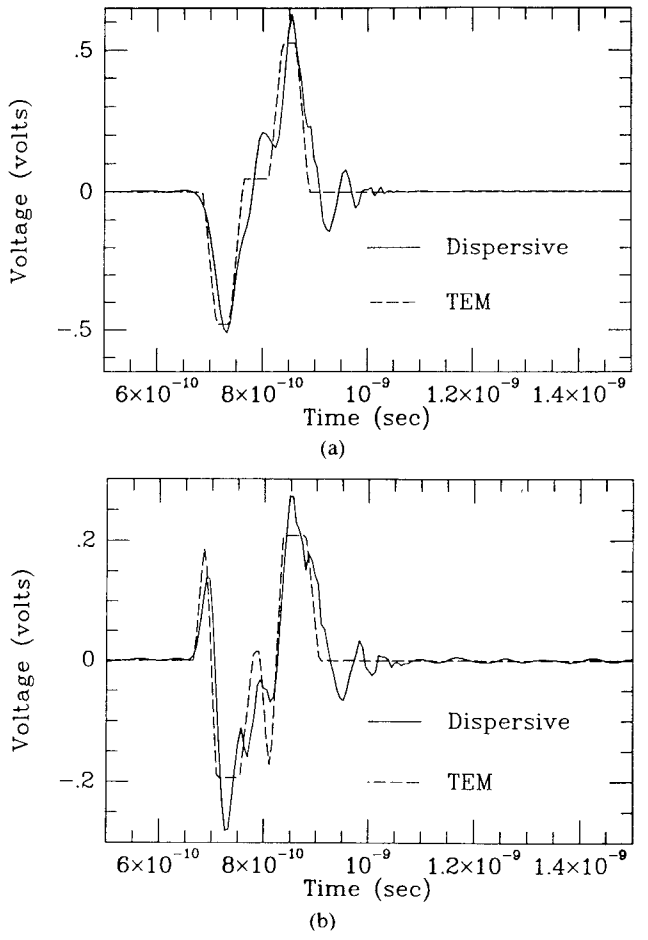

Fig. 5 Isolation results for 7.5-cm-long, 0.254-mm-wide lines on 0.381-mm-thick GaAs substrate. Part (a) is for two lines separated by 0.508 mm and (b) is for three lines separated by 0.127 mm. The terminations are the same as in Fig. 4. Results are plotted for voltages across the capacitors of the coupled line.

each set corresponds to two lines with 0.508 mm separation and part (b) corresponds to two lines with a grounded shield line placed between them on the same plane as the interconnects (for a total of three lines). All of the lines for Figs. 4 and 5 are 0.254 mm wide and a 7.5 cm line length is used for illustrative purposes. For the geometries with an isolation line (case (b) of each set), the strips are separated by 0.127 mm so that the spacing between the two outer lines is 0.508 mm, the same separation as in case (a) of each set (without an isolation line). By comparing the results of (a) and (b) for each set, one can determine how effective (for a given substrate thickness) the presence of the grounded isolation line is in reducing crosstalk. All results are plotted just for the coupled voltage signal because this is of greatest interest when investigating shield lines. A detailed study of the voltage on the driven line is given below in subsection C.

Due to the fast rise and fall times of the source, the effects of dispersion become an issue. One must validate the accuracy of the quasi-TEM approximation by examining the magnitude of the longitudinal fields [20], [21]. In Figs. 4 and 5 results are shown for calculations made using (3) and (4) with and without the effects of dispersion considered. For the results labeled TEM, the same modal effective dielectric constants $((k_{zm}/k_0)^2)$ and values of i_{zlm} and Z_{lm} are used at all frequencies, with parameters calculated at 1 GHz. For the results that considered dispersion, a piecewise-linear approximation was used to simulate the frequency dependence of the effective dielectric constants as well as i_{zlm} and Z_{lm}. The piecewise-linear approximation was made using results calculated with the spectral-domain technique at $f=1,10,20,30,\cdots,90$ GHz. For all frequencies less than 1 GHz, the parameters from the spectral-domain calculation at 1 GHz were used in (3) and (4), since at these frequencies dispersion is negligible. An 8192 point FFT was applied to (3) and (4), and the period of the source was set to 50 ns such that frequency components up to 81.92 GHz are used. Enough terms were taken in the FFT such that the effects of Gibbs' phenomena were negligible. One can see that for the cases considered, the dispersion produces noticeable pulse distortion. This distortion is due mainly to the relatively long lines considered and will be smaller for shorter line lengths.

For thin substrates relative to interline spacing, the fields will reside mainly in the substrate; therefore the effective dielectric constants of the different modes will not differ greatly (they will each be less than but close to the substrate dielectric constant) and minimal crosstalk is expected. The isolation lines should have a lesser effect for thin substrates since the interline coupling should be small even without isolation lines (the effective dielectric constants of the modes are very similar). Conversely, as the substrate thickness becomes large the field lines are less confined between the conductors and ground; therefore a greater range of effective dielectric constants will exist for the various modes. These expectations are confirmed upon examining the two sets of results. For the relatively thin substrate case, Fig. 4(a) and (b), the grounded shield line offers a small reduction in crosstalk. However, for the relatively thick substrates, as in Fig. 5(a) and (b), one sees the grounded isolation line significantly reduces the crosstalk. For thick substrates, the significant reduction in crosstalk obtained using shield lines may justify their use.

The line lengths as well as signal rise and fall time were fixed for all cases considered, but as was shown in Section IV, the rise and fall times as well as line lengths are critical in evaluating isolation line performance. To first order (neglecting dispersion) the variation of the signal rise and fall time for a given line length is the same as varying the line length for fixed signal rise and fall time. The same geometry as analyzed in Figs. 4 and 5 is considered but the substrate thickness is fixed at 0.254 mm. As in Figs. 4 and 5, 7.5 cm line lengths with 20 fF capacitor loads are considered. The rise and fall time of the source is varied from 10 to 500 ps, and the maximum voltage crosstalk is calculated at the terminations (capacitors). Dispersion is accounted for by solving the boundary value problem using the spectral-domain technique as described above. The results are plotted in Fig. 6 as a function of rise and fall time with and without grounded isolation lines. It is seen that for this geometry, the grounded isolation line

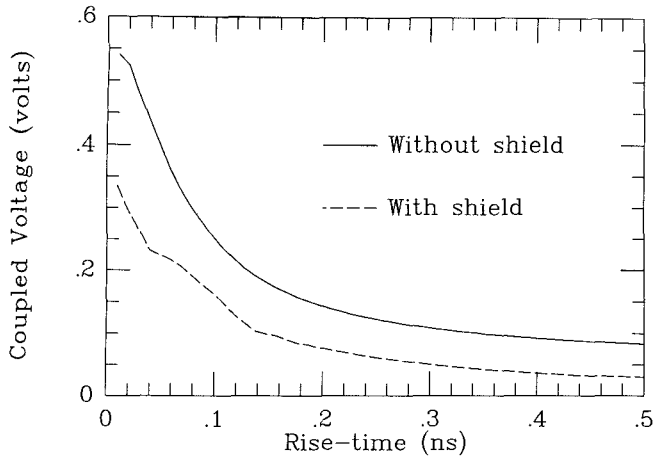

Fig. 6. Maximum absolute value of coupled voltage as a function of signal rise time. The lines are on a 0.254-mm-thick GaAs substrate. The line lengths, widths, separations, and terminations are the same as those used in Figs. 4 and 5 for lines with and without a grounded isolation line. One outer line is driven with a 1 V, 1-ns-wide pulse.

reduces the crosstalk for all signal rise times. However, for the relatively slow rise times the crosstalk is small even without an isolation line and therefore the added fabrication complexity associated with the grounded isolation line may not be warranted.

B. Si–SiO_2 Substrate

Consider the three line, dual-level geometry in Fig. 1 with dielectric constants $\epsilon_{r1}=1$, $\epsilon_{r2}=4$ (SiO_2), and $\epsilon_{r3}=12$ (Si). Over the SiO_2 insulating surface lie two interconnects with a shield line residing on the Si–SiO_2 interface. Configurations similar to this are feasible with current fabrication techniques. Because the shield line is not on the same level as the interconnects, it may allow smaller interline spacing for the interconnects (as compared to having the shield on the interconnect level) and therefore lends itself to more densely packaged circuits. The two top lines are 10 μm wide, the silicon is 250 μm thick, and the square shield box has 500 μm sides. One of the interconnects is excited with a unit-amplitude, 0.1-ns-rise-time (0 to 100%) current pulse with 1 ns width (at peak) and the currents at the source end of the nondriven lines are set to zero. The currents on the lines are calculated as a function of position for several interconnect separations s and SiO_2 thicknesses d. Fig. 7 shows results when there is no isolation line and Fig. 8 shows results for the addition of a 10-μm-wide isolation line on the Si–SiO_2 interface. The results were calculated using (3) in conjunction with the FFT ($a_m^{(-)}=0$). Dispersion was found to be negligible for a 0.1 ns pulse on this structure and was therefore not considered in these calculations.

The conclusions from these results are that for relatively long lines (> 30 mm) the reduction in crosstalk caused by the isolation line is appreciable for 0.1-ns-rise-time pulses on the structures considered. However for short line lengths, although the isolation line reduces crosstalk, the interline coupling is so small as to most likely not be of importance. An interesting fact can be seen by considering the results in Fig. 7: the crosstalk with no isolation line can be significantly reduced by just increasing the SiO_2 thickness. This is because for thick SiO_2, more of the fields are in the air and SiO_2 regions (away from the high-dielectric-constant silicon substrate) and therefore there is a smaller range of possible values for the modal effective dielectric constants. Note that for the single-layered GaAs substrate considered in subsection A the crosstalk increased with larger substrate thickness while for the dual-layered Si–SiO_2 substrate the increased SiO_2 thickness reduced the crosstalk. Although the conclusions are different in the two cases, the argument is the same in both: the wider the range of modal effective dielectric constants, the greater the expected crosstalk for a given line length and signal speed.

C. Isolation Line Drawbacks

It has been mentioned that the use of grounded isolation lines increases fabrication complexity. In this subsection another possible drawback of grounded isolation lines is investigated. Consider the Si–SiO_2 geometry studied in subsection B with $t=250$ μm, $w_1=w_2=d=10$ μm, and $s=20$ μm. Fig. 9 shows results for line 1 driven by a 1 V, 50 ps rise (0 to 100%) and fall time pulse of 100 ps width (at peak). The source impedance is 50 Ω. Line 2 is not driven and has a 50 Ω impedance at its input port; lines 1 and 2 are terminated in 0.5 pF capacitors at the load end; the lines are 20 mm long; and line 3 is not present. Fig. 10 considers the geometry of Fig. 9 with the addition of a grounded isolation line (strip 3 with $w_3=10$ μm) on the Si–SiO_2 interface. Dispersion was accounted for in the computation of Figs. 9 and 10 in the same manner as was done for the calculations of dispersive pulse propagation on the GaAs substrates considered in subsection A. One notices that the isolation line successfully reduces the crosstalk to the nondriven signal line at both the generator and load ends. However, the addition of the isolation line significantly increases the amplitude of the return voltage pulse at the generator end of the driven line. It should be noted that the large return signal on the driven line was also observed for pulse propagation on the single-layered GaAs substrates studied in subsection A (with an isolation line) although the signal on the nondriven line was reduced at both ports. A check was made to see how this phenomenon is affected by the port terminations by considering 50 Ω terminations at the load end instead of capacitors (while all other line characteristics and boundary conditions remain unchanged), and the increased return signal at the generator end of the driven line was still observed when the shield line was used. The coupled signal at the load end of the nondriven line was smaller with the isolation line than without. However, in agreement with [4], the return signal at the generator end of the nondriven line was also higher with the isolation line than without for the 50 Ω termination case. For the case of 50 Ω load impedances terminating the interconnects, without the grounded shield line the 50 Ω terminations at the output ports provide a relatively good match to the lines, and the

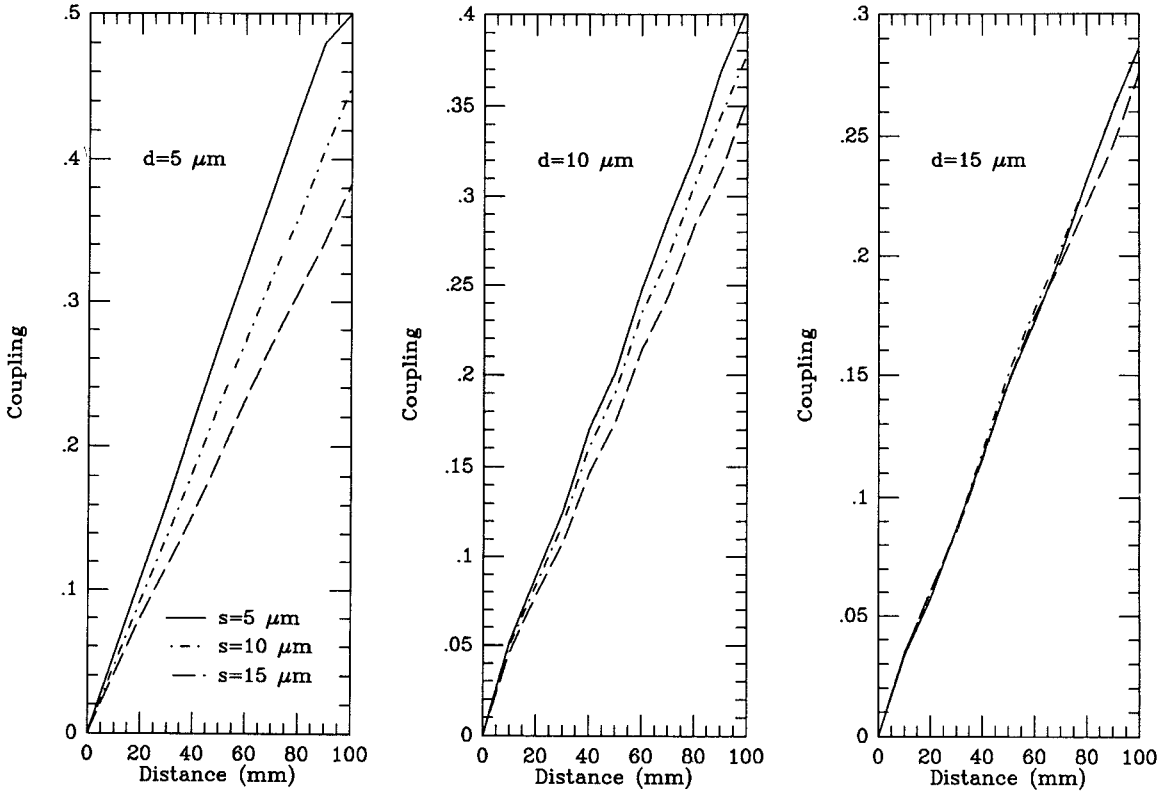

Fig. 7. Maximum absolute value of relative coupling to line 2 of Fig. 1 with a 0.1-ns-rise-time pulse driving line 1. The semi-infinite lines have $w_1 = w_2 = 10$ μm, $t = 250$ μm, $a = h = 500$ μm, and line 3 is not present. The dielectric constants are $\epsilon_{r1} = 1$, $\epsilon_{r2} = 4$, and $\epsilon_{r3} = 12$. The three graphs are for $d = 5$, 10, and 15 mm.

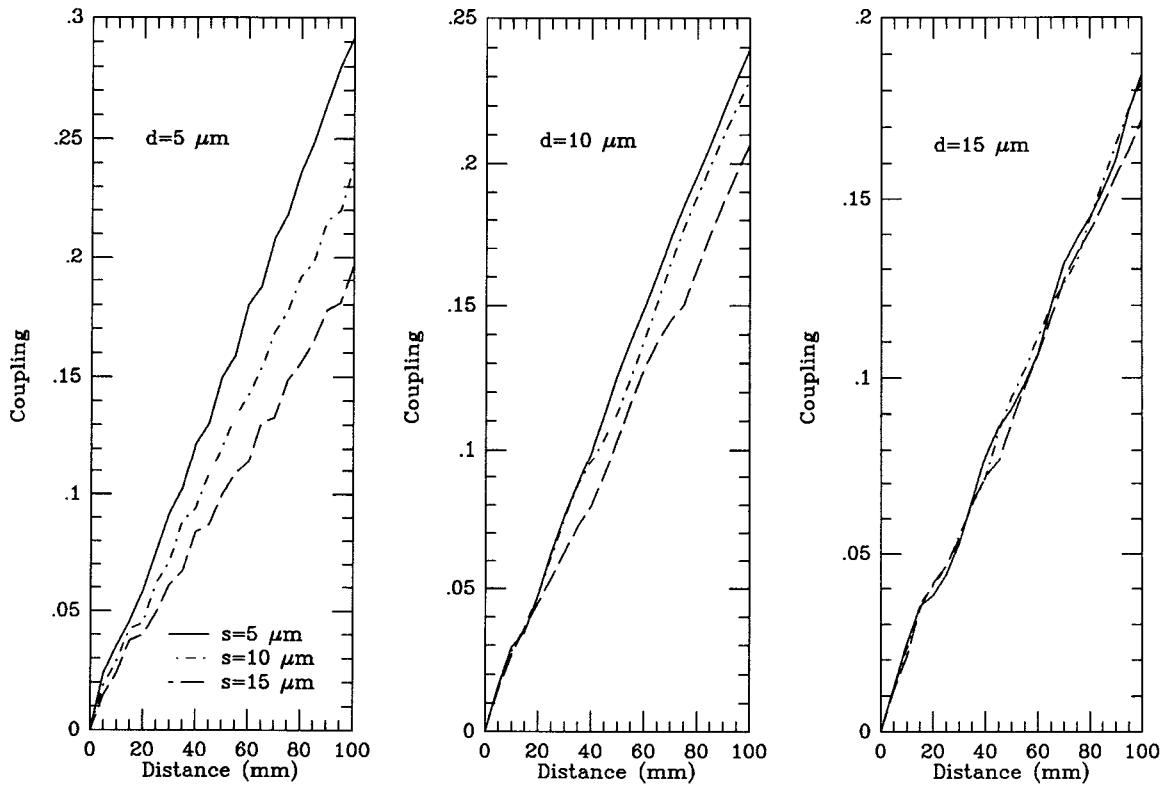

Fig. 8. Maximum relative coupling to line 2 of Fig. 1 with a 0.1-ns-rise-time pulse driving line 1 with an isolation line present. The geometry is the same as that in Fig. 7 except $w_3 = 10$ μm.

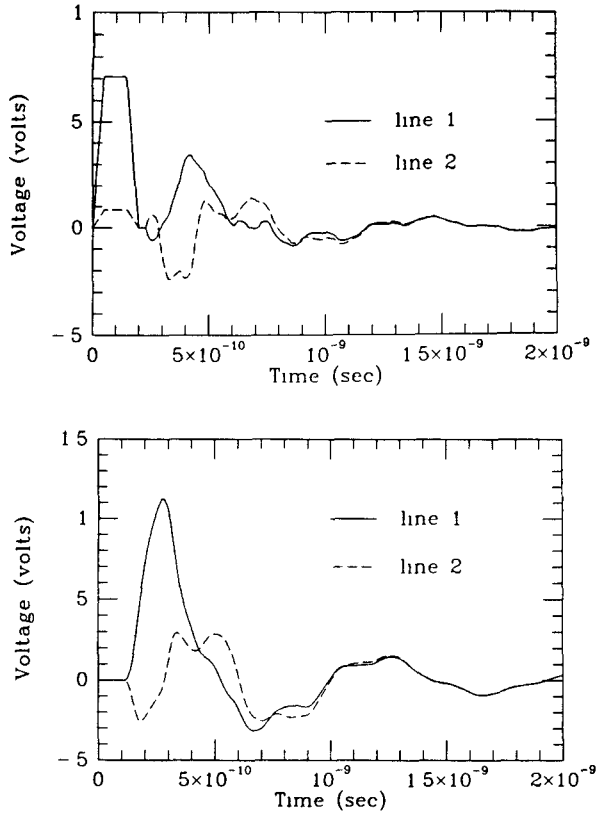

Fig. 9. Pulse response for microstrip in Fig. 1 with line 3 not present. Geometrical parameters: $w_1 = w_2 = d = 10\ \mu$m, $t = 250\ \mu$m, $s = 20\ \mu$m, and 20 mm line lengths. Line 1 is driven by a 1 V, 50 ps rise (0 to 100%) and fall time pulse of 100 ps width (at peak). Lines 1 and 2 have 50 Ω impedances at the generator end and are terminated in 0.5 pF capacitors at the load end. The top curve corresponds to the voltage at the source end, and the bottom figure is for the load end.

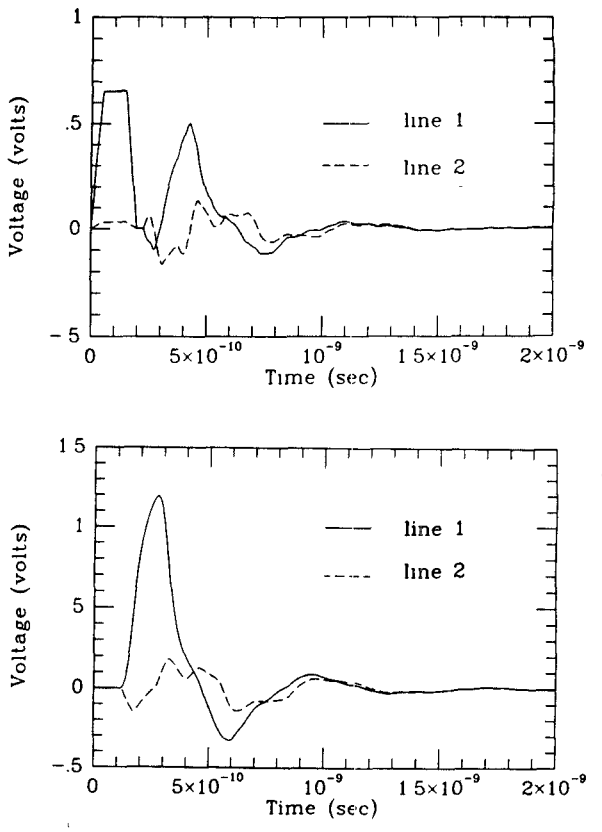

Fig. 10. Pulse response for the same geometry as in Fig. 9 with the addition of a grounded shield line (strip 3 in Fig. 1). The excitation and boundary conditions on lines 1 and 2 are the same as in Fig. 9. The top curve corresponds to the voltage at the source end, and the bottom figure is at the load end.

reflected pulse on line 1 is relatively small. However, with the addition of the grounded shield line the boundary conditions on the output ports of the lines change such that now the match is no longer as good and a larger pulse is reflected back on line 1. For some cases this large reflected signal will couple enough to the nondriven line on the return to the generator end to actually increase the return voltage at the generator end of the nondriven line (compared to the voltage present without the shield). A similar argument can be made regarding the effect of the boundary conditions at the source end, resulting in possible pulse ringing.

VI. Summary

A full-wave-based technique has been used to study multiline interconnects and to address the effectiveness of grounded isolation or shield lines in reducing crosstalk in interconnects. It was shown that the effectiveness of such lines depends on several factors, the most important of which are relative mode velocities, signal rise and fall times, and line length. Grounded isolation lines were considered for single-layered strips on a GaAs substrate and for dual-level strips in a Si–SiO_2 environment. By placing the isolation line on a different level than the interconnects (in the Si–SiO_2 case) greater packaging density can be achieved. The isolation lines were found to be effective in reducing crosstalk to the load end of the nondriven line for all cases considered: various substrate thicknesses and signal speeds for the GaAs geometry, and various line lengths and SiO_2 thicknesses for the Si–SiO_2 geometry. However, for many cases (slow rise and fall times, short line lengths, and/or weakly coupled lines) it was shown that the crosstalk to the nondriven line is very small without the isolation line and therefore the need for the shield line may not be justified. This is in light of the fact that the grounded isolation line significantly increases fabrication complexity and may cause an increase in the signal at the generator end of the lines. For the Si–SiO_2 geometry it was also shown that crosstalk can be reduced significantly without a shield line by increasing the SiO_2 thickness.

References

[1] S. Seki and H. H. Hasegawa, "Analysis of cross-talk in very high-speed LSI/VLSI's using a coupled multiconductor MIS microstrip line mode," *IEEE Trans. Microwave Theory Tech.*, vol. MTT-32, pp. 1715–1718, Dec. 1984.

[2] J. Chilo and T. Arnaud, "Coupling effects in the time domain for an interconnecting bus in high-speed GaAs logic circuits," *IEEE Trans. Electron Devices*, vol. ED-31, pp. 347–352, Mar. 1984.

[3] J. Chilo, C. Monllor, and M. Bouthinon, "Interconnection effects in fast integrated GaAs circuits," *Int. J. Electron.*, vol. 58, pp. 671–686, Apr. 1985.

[4] A. R. Djordjevic, T. K. Sarkar, and R. F. Harrington, "Time-domain response of multiconductor transmission lines," *Proc. IEEE*, vol. 75, pp. 743–764, June 1987.
[5] J. A. DeFalco, "Reflection and cross-talk in logic circuit interconnects," *IEEE Spectrum*, pp. 44–50, July 1970.
[6] F. Chang, "Transient analysis of lossless coupled transmission lines in a nonhomogeneous medium," *IEEE Trans. Microwave Theory Tech.*, vol. MTT-18, pp. 616–626, Sept. 1970.
[7] F. Chang, "Computer-aided characterization of coupled TEM transmission lines," *IEEE Trans. Circuits Syst.*, vol. CAS-27, pp. 1194–1205, Dec. 1980.
[8] V. K. Tripathi and J. B. Retting, "A SPICE model for multiple coupled microstrips and other transmission lines," *IEEE Trans. Microwave Theory Tech.*, vol. MTT-32, pp. 1513–1518, Dec. 1985.
[9] A. R. Djordjevic, T. K. Sarkar, and R. F. Harrington, "Analysis of lossy transmission lines with arbitrary nonlinear terminal networks," *IEEE Trans. Microwave Theory Tech.*, vol. MTT-34, pp. 660–666, June 1986.
[10] R. F. Harrington and C. Wei, "Losses on multiconductor transmission lines in multilayered dielectric media," *IEEE Trans. Microwave Theory Tech.*, vol. MTT-32, pp. 705–710, July 1984.
[11] R. E. Diaz, "The discrete variational conformal technique for the calculation of strip transmission line parameters," *IEEE Trans. Microwave Theory Tech.*, vol. MTT-34, pp. 714–722, June 1986.
[12] E. G. Farr, C. H. Chan, and R. Mittra, "A frequency-dependent coupled-mode analysis of multiconductor microstrip lines with applications to VLSI interconnection problems," *IEEE Trans. Microwave Theory Tech.*, vol. MTT-34, pp. 307–310, Feb. 1986.
[13] Y. Fukuoka, Q. Zhang, D. P. Neikirk, and T. Itoh, "Analysis of multilayer interconnection lines for a high-speed digital circuit," *IEEE Trans. Microwave Theory Tech.*, vol. MTT-33, pp. 527–532, June 1985.
[14] T. Itoh, "Spectral domain immitance approach for dispersion characteristics of generalized printed transmission lines," *IEEE Trans. Microwave Theory Tech.*, vol. MTT-28, pp. 733–736, July 1980.
[15] D. Mirshekar-Syahkal and J. B. Davies, "Accurate solution of microstrip and coplanar structures for dispersion and for dielectric and conductor losses," *IEEE Trans. Microwave Theory Tech.*, vol. MTT-27, pp. 694–699, July 1979.
[16] R. H. Jansen, "Unified user-oriented computation of shielded, covered and open planar microwave and millimeter-wave transmission characteristics," *Proc. Inst. Elec. Eng.*, pt. H, vol. MOA 1, pp. 14–22, 1979.
[17] L. Weimer and R. H. Jansen, "Reciprocity related definition of strip characteristic impedance for multiconductor hybrid-mode transmission lines," *Microwaves and Opt. Technol. Lett.*, vol. 1, pp. 22–25, Mar. 1988.
[18] L. Carin and K. J. Webb, "Characteristic impedance of multi-level, multiconductor hybrid mode microstrip," *IEEE Trans. Magn.*, July 1989.
[19] J. R. Brews, "Transmission line models for lossy waveguide interconnections in VLSI," *IEEE Trans. Electron Devices*, vol. ED-33, pp. 1356–1365, Sept. 1986.
[20] L. Carin and K. J. Webb, "An equivalent circuit model for terminated hybrid-mode multiconductor transmission lines," *IEEE Trans. Microwave Theory Tech.*, vol. 37, pp. 1784–1793, Nov. 1989.
[21] J. R. Mosig and T. K. Sarkar, "Comparison of quasi-TEM and exact electromagnetic fields from a horizontal dipole above a lossy dielectric backed by an imperfect ground plane," *IEEE Trans. Microwave Theory Tech.*, vol. MTT-34, pp. 379–387, Apr. 1986.

✠

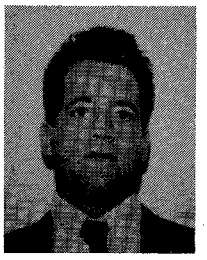

Lawrence Carin was born in Washington, DC, on March 25, 1963. He received the B.S., M.S., and Ph.D. degrees, all in electrical engineering, from the University of Maryland, College Park, in 1985, 1986, and 1989, respectively.

He is now an Assistant Professor with the Electrical Engineering Department at the Polytechnic Institute of New York. His present research interests include the analysis of electromagnetic waves in planar and quasi-planar structures used in high-speed integrated circuits. Dr. Carin is a member of Tau Beta Pi and Eta Kappa Nu.

✠

Kevin J. Webb (S'81–M'84) was born in Stawell, Victoria, Australia, on July 7, 1956. He received the B.Eng. and M.Eng. degrees from the Royal Melbourne Institute of Technology, Australia, in 1978 and 1983, respectively, the M.S.E.E. degree from the University of California, Santa Barbara, in 1981, and the Ph.D. degree in electrical engineering from the University of Illinois, Urbana, in 1984.

From 1984 until 1989 he was an Assistant Professor in the Electrical Engineering Department at the University of Maryland, College Park, and since January 1990 he has been an Associate Professor in the School of Electrical Engineering at Purdue University, West Lafayette, IN. His research interests include microwave and millimeter-wave integrated circuits, VLSI circuits, optoelectronics, numerical electromagnetics, and frequency selective surfaces.